Accepted for publication in Proc. MICCAI Workshop on Multimodal Learning and Fusion Across Scales for Clinical Decision Support
The final authenticated version will be published by Springer.

Predicting Treatment Response in Prostate Cancer Patients Based on Multimodal PET/CT For Clinical Decision Support

Sobhan Moazemi[1,2][0000−0003−3277−3596], Markus Essler[2], Thomas Schultz[1,3][0000−0002−1200−7248], and Ralph A. Bundschuh[2]

[1] Department of Computer Science, University of Bonn, 53115 Bonn, Germany
[2] Department of Nuclear Medicine, University Hospital Bonn, 53127 Bonn, Germany
{s.moazemi,markus.essler,ralph.bundschuh}@ukbonn.de
[3] Bonn-Aachen International Center for Information Technology (BIT), 53115 Bonn, Germany
schultz@cs.uni-bonn.de

Abstract. Clinical decision support systems (CDSSs) have gained critical importance in clinical practice and research. Machine learning (ML) and deep learning methods are widely applied in CDSSs to provide diagnostic and prognostic assistance in oncological studies. Taking prostate cancer (PCa) as an example, true segmentation of pathological uptake and prediction of treatment outcome taking advantage of radiomics features extracted from prostate-specific membrane antigen-positron emission tomography/computed tomography (PSMA-PET/CT) were the main objectives of this study. Thus, we aimed at providing an automated clinical decision support tool to assist physicians. To this end, a multi-channel deep neural network inspired by U-Net architecture is trained and fit to automatically segment pathological uptake in multimodal whole-body baseline ^{68}Ga-PSMA-PET/CT scans. Moreover, state-of-the-art ML methods are applied to radiomics features extracted from the predicted U-Net masks to identify responders to ^{177}Lu-PSMA treatment. To investigate the performance of the methods, 2067 pathological hotspots annotated in a retrospective cohort of 100 PCa patients are applied after subdividing to train and test cohorts. For the automated segmentation task, we achieved 0.88 test precision, 0.77 recall, and 0.82 Dice. For predicting responders, we achieved 0.73 area under the curve (AUC), 0.81 sensitivity, and 0.58 specificity on the test cohort. As a result, the facilitated automated decision support tool has shown its potential to serve as an assistant for patient screening for ^{177}Lu-PSMA therapy.

Keywords: Clinical Decision Support System · Machine Learning · Deep Learning · Multimodal Imaging · Positron Emission Tomography · Computed Tomography · Prostate Cancer

1 Introduction

Computer-aided diagnosis (CAD) has been used extensively to assist physicians and researchers in a variety of fields including oncology. Prostate cancer endangers men's health as the fifth cancer disease to cause mortality in the world [1].

To assess the disease stage as well as to monitor the treatment progress, PET/CT scans are commonly used. PET/CTs are multimodal medical imaging techniques which are widely used for different cancer diseases [2–4, 12]. On the one hand, PET scans outline differences in functional activities of different tissues. On the other hand, CT scans provide high-resolution spatial and anatomical information of the tissues. Thus together, PET and CT provide both functional and anatomical information to locate malignancies.

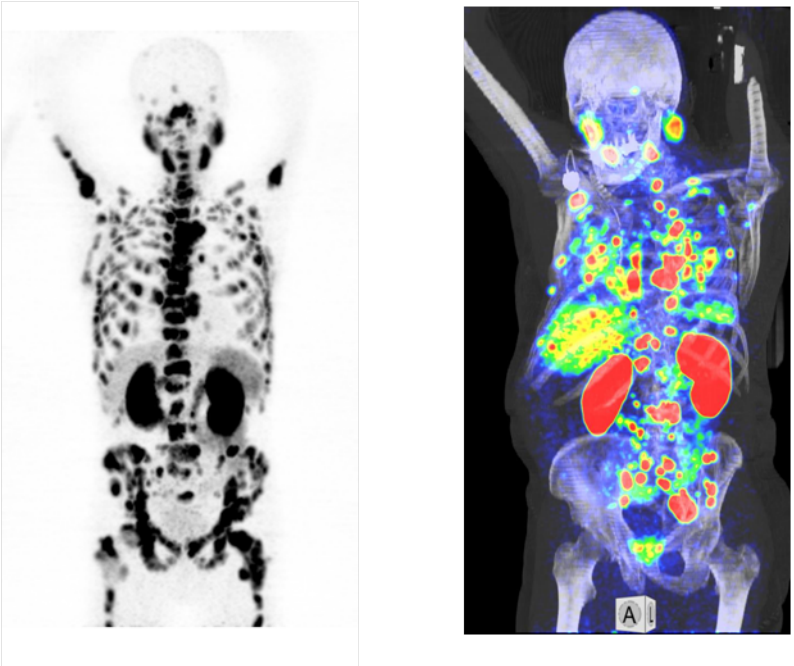

Fig. 1. An example of multimodal imaging for prostate cancer management. Left: the positron emission tomography (PET), right: the overlaid PET/computed tomography (PET/CT). The red uptake in the right panel includes both pathological and physiological uptake.

In clinical routine, nuclear medicine (NM) physicians often spend an enormous amount of time to analyze medical imaging modalities to locate cancerous tissues and to stage the disease. Moreover, considering the treatment expenses, avoiding unnecessary treatment would be of critical importance. Thus, on the one hand, clinical decision support tools can reduce the time and effort required by the domain experts, and on the other hand, they could help with identifying the patients who might not benefit from the therapy in a timely manner.

In order to make diagnostic and prognostic decisions based on PET/CT scans, several issues need to be taken care of. First of all, PET and CT scans,

even when taken with the same scanner, are produced in different resolutions and often in different coordination systems. Second of all, as a non-invasive diagnostic method, true segmentation of pathological (i. e., malignant) uptake is of critical importance. Last but not least, the required time and effort to conduct decisive actions need to be minimized. To tackle the first challenge, co-registration and resampling of the two modalities and bringing them to the same coordinate system have to be conducted. Furthermore, for the segmentation of the malignant tissues, appropriate labeling and annotation tools should be applied. Finally, to optimize the whole diagnostic procedure in terms of time and effort, (semi-) automated assistant tools need to be provided. The main contribution of our methods is to provide such an automated tool which facilitates both the automated segmentation of pathological uptake as well as the identification of non-responders to therapy.

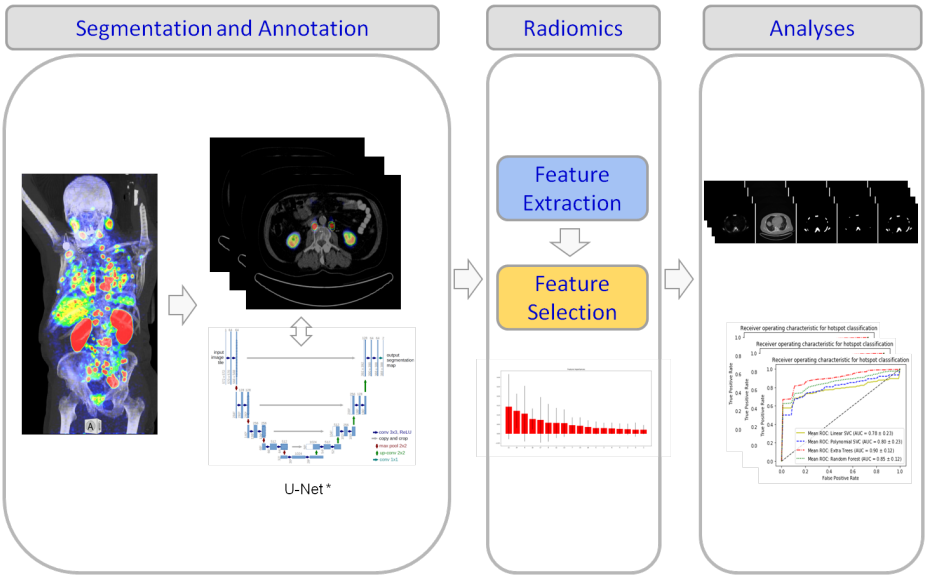

Fig. 2. The high-level outline of the tools. The segmentation and annotation module consists of in-house developed and third party software for automatic and manual segmentation and labeling of the input scans. The radiomics unit utilizes radiomics feature calculation and selection. The analyses module encapsulates the tools used for the visualization of study results (*: the original U-Net architecture as proposed by Ronneberger et al. [8]).

In general, given PET 3D scans, cancerous and metastatic tissues usually feature higher metabolic uptake than benign or normal tissues. However, challenges arise as some organs such as liver and kidneys also associate with high uptake which is considered as not pathological (i. e., physiological). Thus, discriminating pathological uptake becomes more challenging for inexperienced annotators.

To cope with this issue, often CT scans complement PET scans as an additional channel to better locate the sites with pathological uptake. Figure 1 illustrates an example of multimodal PET/CT scans, denoting the similarities between pathological and physiological uptakes.

As conventional segmentation methods, thresholding based algorithms are applied to PET scans, leveraging fixed and adaptive thresholds such as 40% of maximum standardized uptake values (40%-SUV$_{MAX}$). However, inconsistencies in scanning resolutions and protocols from scanner to scanner and from center to center expose limitations to thresholding based approaches. To address this issue, automated segmentation leveraging deep neural networks have been beneficial in many diagnostics fields such as oncology [5], drusen segmentation [6] and computational neuroscience [7]. Since first time proposed by Ronneberger et al. [8], U-Net based architectures have been widely applied in medical domain for different segmentation tasks [9, 10]. Liu et al. [11] have conducted a survey on U-shaped networks used for medical image segmentation.

As the next consecutive step towards diagnosis and therapy response prediction, deep and supervised ML methods are commonly used in combination with radiomics analyses in clinical research [12–14]. The term radiomics denotes the procedure of extracting numerical quantities out of medical imaging data in terms of two or three dimensional (2D or 3D) intensity, shape, or texture based features which characterize tumors and other hotspots.

In this manuscript, we introduce a clinical decision support tool consisting of an automated segmentation unit inspired by U-Net architecture and supervised ML classifiers to distinguish responders and non-responders to ^{177}Lu-PSMA as a routine therapy procedure to treat patients diagnosed with prostate cancer. The presented automated tools facilitate the management of PCa patients based on baseline ^{68}Ga-PSMA-PET/CT scans. To end up with the ultimate decision support solution, several steps are taken: 1) preprocess and resample PET and CT input Dicom [15] images, 2) annotate the input images to provide ground truth (GT) labels for ML and deep learning pipelines, 3) automatically segment the pathological uptake using deep neural networks (NNs) and extract radiomics features based on the predicted masks, 4) utilize supervised ML classifiers to predict the responders to therapy based on the radiomics features extracted from the PET/CT findings.

For this study, a cohort of 100 PCa patients have been retrospectively analyzed and subdivided to training and test cohorts as detailed in Section 2.2. The training cohort is used for training and fitting the automated segmentation pipeline and for training and hyperparameter tuning of the supervised ML classifiers as used for therapy response prediction. We took advantage of TensorFlow [16] and Keras [17] libraries to customize our U-Net based segmentation model based on multimodal PET and CT channels to predict masks based on manually annotated GT masks using third party software. Dice coefficient [18] is applied to quantify the amount of agreement between the predicted masks and the given GT masks. As a result, the superiority of combination of PET and CT channels compared to masks predicted using only PET channel is shown. In the next step,

PyRadiomics library [19] is used to calculate the radiomics features for PET and CT modalities based on the pathological uptake predicted by the implemented PET-CT-U-Net. In the final step, ML classifiers are applied to the calculated radiomics features to predict responders to therapy. This step includes recursive feature elimination (RFE) technique [20] to identify the most relevant features for the classification problem.

To the best of our knowledge, so far, no other automated clinical decision support tool based on deep learning methods is presented for the management of prostate cancer patients using baseline ^{68}Ga-PSMA-PET/CT findings.

2 Methods

2.1 Pipeline Overview

The study pipeline consists of several modules including multimodal PET/CT resampling and visualization tool box, U-Net based segmentation, radiomics feature extraction and selection, and prognosis which together serve as a clinical decision support system (CDSS) for the management of PCa patients. Figure 2 gives a high-level outline of the tools. The whole pipeline is represented as three consecutive building blocks: 1) segmentation and annotation, 2) radiomics, and 3) analyses.

The segmentation and annotation block consists of various assets facilitating manual and automated segmentation and annotation of multimodal PET/CT images. For instance, InterView FUSION [21] is used for the manual delineation of hotspots while an in-house developed deep segmentation network based on U-Net [8] is used for automated segmentation of pathological uptake. The radiomics block consists of feature extraction and selection tools. Finally, the analyses block covers the tools and diagrams aiming at representing the end-user level analyses and insights.

Table 1. The summary of the clinical information of the patients cohort (PSA: prostate specific antigen).

	Age [years]	**Gleason Score**	**PSA [ng/ml]**
Minimum	48	6	0.25
Maximum	87	10	5910
Average	70.40	8.32	461.57

2.2 Dataset and Ground Truth Annotation

For this study, a cohort of 100 patients (67 responders vs 33 non-responders) who had been diagnosed with advanced prostate carcinoma and had been selected for ^{177}Lu-PSMA therapy has been analyzed retrospectively. The patients' ages

ranged from 48 to 87 years. Table 1 gives an overview of the clinical information of the cohort. A Biograph 2 PET/CT system (Siemens Medical Solutions, Erlangen, Germany) was used for image acquisition and reconstruction. A random subset of 61 subjects (40 responders vs 21 non-responders) is used for training, while the rest of the patients (39 patients including 27 responders and 12 non-responders) have served as test cohort. All patients gave written and informed consent to the imaging procedure and for anonymized evaluation of their data. Due to the retrospective character of the data analysis, an ethical statement was waived by the institutional review board according to the professional regulations of the medical board of the state of North-Rhine Westphalia, Germany.

To provide ground truth (GT) labels for the ML based pipeline, a team of NM physicians supervised by a highly qualified NM expert with 7 years of practical experience in PET/CT diagnosis analyzed and annotated the whole dataset using InterView FUSION. In a previous study [27], we have analyzed the inter-observer variability aspects of GT annotation. The dataset is annotated in a slice-based manner. Thus, each pathological hotspot was delineated as several consecutive 2D regions of interest (RoIs) in subsequent slices, together forming the volumes of interest (VoIs). On average, 20 pathological hotspots have been identified for each patient (in total, 2067 pathological hotspots). The pathological hotspots include primary uptake in prostate as well as metastatic uptake in other organs such as bone and lymph nodes.

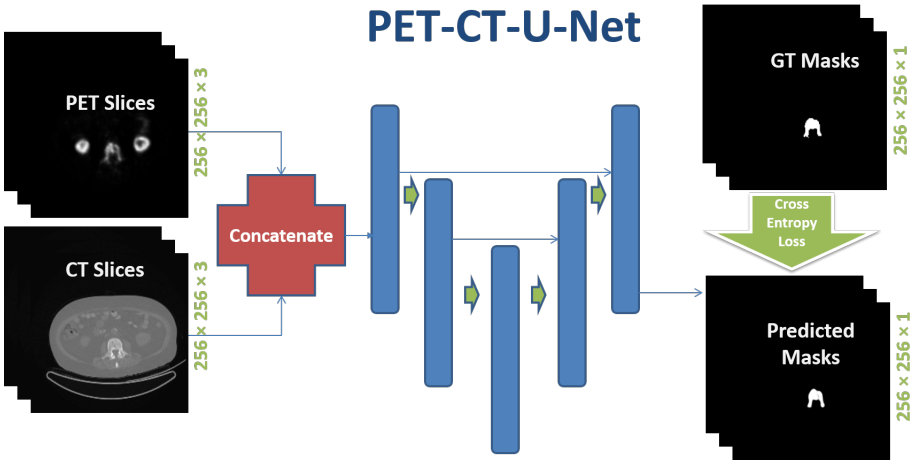

Fig. 3. The simplified schematic of the implemented multimodal U-Net based segmentation network (PET-CT-U-Net). PET and CT slices are processed as separate channels. Two alternative models are applied: PET only, and PET/CT. Weighted binary cross-entropy serves as the loss function.

2.3 Automated Segmentation

The U-Net based segmentation unit, inspired by a single channel U-Net model implemented for polyp segmentation [22], is a multi-channel network which takes resampled images from original Dicom format PET and CT images as 2D sliced input. In addition, the 2D sliced manually delineated GT masks are used as GT labels. Also, the network internally creates the threshold based 40%-SUV$_{MAX}$ masks from PET for quantitative as well as qualitative comparison. The segmentation network defines two different models based on input channels: single and dual. The simplified architecture of the automated segmentation network is illustrated in figure 3.

In the first training step, the U-Net based model is trained and fit using PET and the combinations of PET and CT. As a result, two alternative models are trained, a model based on only PET and a model based on both PET and CT images respectively. The 40%-SUV$_{MAX}$ masks are used to set a baseline for performance analysis of the segmentation network. The U-Net model, developed in Python V.3.6 and utilized TensorFlow and Keras libraries, consists of encoding and decoding steps connected via a bridge layer. The input image sizes are set to 256256 and the filter numbers are as follows: 16, 32, 48, 64, 128, 256, 480, 512. Thus, we customize the resolution levels compared to the original U-Net architecture. By looping over the filter numbers and applying a 2D convolution block followed by a 2D max pooling at each iteration, the encoding step is taken. Then the bridge layer comes to action by applying a single 2D convolution block. Afterwards, the decoding step loops over the reversed filter numbers and applies a 22 upsampling followed by a 2D convolution block at each iteration. Finally, a sigmoid activation layer is applied after 11 2D convolution to end up with the output binary image. The 2D convolution block is composed of two 33 convolutions, each consisting of a batch normalization and a rectified linear unit (ReLU) activation.

Due to the imbalance in the number of pixels in GT masks and background and because the outputs of the network are predicted binary images, weighted binary cross entropy is selected as the loss function. The segmentation quality metric is measured as the Dice coefficient of the predicted and GT masks. The networks are further tuned with different values for hyperparameters such as batch size (values: 8 and 16), learning rate (values: 0.0001, 0.001, 0.01, and 0.1), and up to 60 epochs. First, the train_test_split function of the model_selection class of Scikit-Learn library is applied to subdivide the training cohort into interim train and validation subsets. Consecutively, the Dice coefficient of the predicted masks and GT labels (encoded as 2D binary images) is determined to fit the model. This process is repeated until the maximum number of epochs is reached or the early stopping criteria (using TensorFlow's EarlyStopping function with inputs: monitor=validation_loss and patience=10) are met. Then, the fitted model is used to predict the masks for the held-out test set. Finally, the generated masks will be analyzed quantitatively (using Dice coefficients) as well as qualitatively (by the experienced NM expert). To prepare the input dataset for the therapy response prediction, the best predicted mask is used to calculate

radiomics features. To this end, for each patient, the predicted mask is applied to input images to calculate features using PyRadiomics library and end up with patient-specific feature vectors.

2.4 Therapy Response Prediction

Once the radiomics features are generated from the segmentation unit, 6 different ML classifiers (logistic regression [23], support vector machine (SVM) [24] with linear, polynomial and radial basis function (RBF) kernels, extra trees [25] and random forest [26]) are used for the task of prediction of responders to ^{177}Lu-PSMA treatment. We further analyze the radiomics features and apply recursive feature elimination to end up with the most relevant features to the classification problem. Here, the same training cohort of 61 subjects as used for the training of the segmentation network is applied for training and hyperparameter tuning in a cross validation (CV) step. For the CV, stratified KFold is used with 3 folds. In each CV step, the train and validate feature vectors are standardized using MinMax standardization method. For the hyperparameter tuning, grid search is applied for all of the classifiers based on standard possible ranges of each hyperparameter such as C and Gamma for the SVM classifiers and max_depth and min_sample_leaf for the decision tree based classifiers. For example, the hyperparameter C ranged from 2^{-5} to 2^{15} and min_sample_leaf ranged from 1 to 10. In the final step, the performance of each classifier is measured as applied to the feature vectors from the held-out test cohort. The performances are quantified as area under the receiver operating characteristic (ROC) curve (AUC), sensitivity (SE), and specificity (SP). As the baseline for comparison, the classifiers performances are quantified as the GT mask is applied for the calculation of radiomics features using PyRadiomics library.

Table 2. The performances of different U-Net based segmentation models as trained and fit with the training cohort and applied to the test cohort. The performance of 40%-SUV$_{MAX}$ mask has been quantified for comparison. The precision, recall and Dice values are mean and standard deviations over the test subject cohort. (lr: learning rate, acc: accuracy).

Model/Mask	epochs	lr	acc	dice	loss	precision	recall
40%-SUV$_{MAX}$	–	–	99	39.62 ± 16.6	0.01	38.53 ± 21.38	51.48 ± 19.19
PET (Single)	35	0.001	99	71.51 ± 4.9	0.01	83.63 ± 5.3	63.38 ± 4.8
PET/CT (Dual)	32	0.001	99	82.18 ± 4.7	0.01	88.44 ± 4.8	77.09 ± 5.7

3 Results

3.1 Segmentation

As described in Methods section, we analyzed both singular (i. e. just PET) and multiple (PET + CT) input channels to train and fit our segmentation model.

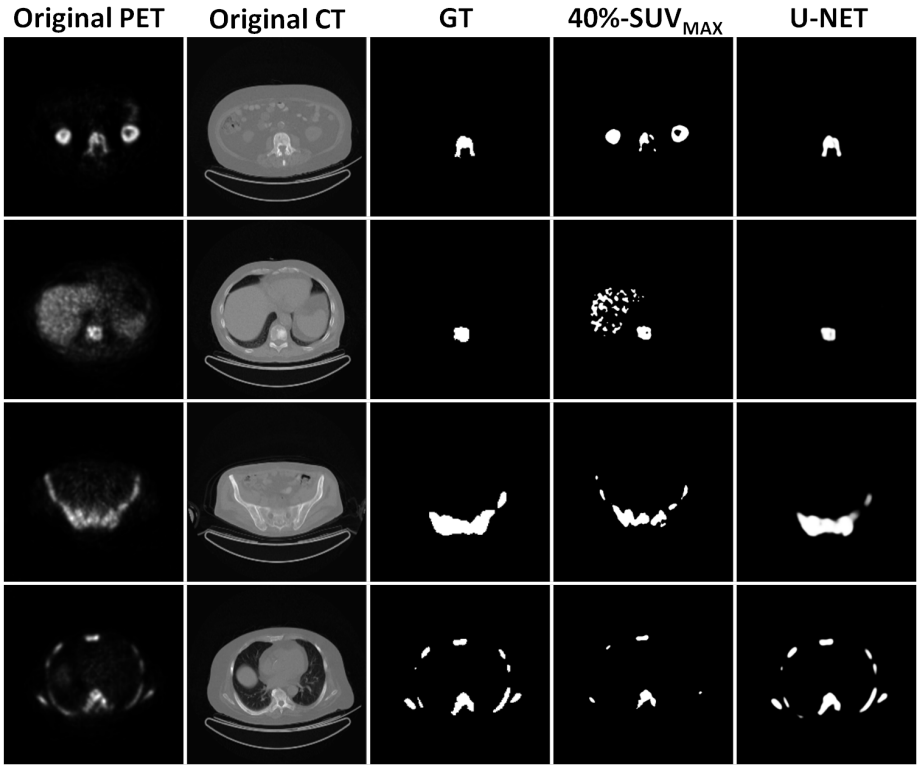

Fig. 4. Example slices of the U-Net based segmentation results. The input PET and CT slices, the ground truth (GT), 40%-SUV$_{MAX}$ PET, and predicted masks are shown. The rows belong to unique 2D slices from arbitrary subjects of the test cohort.

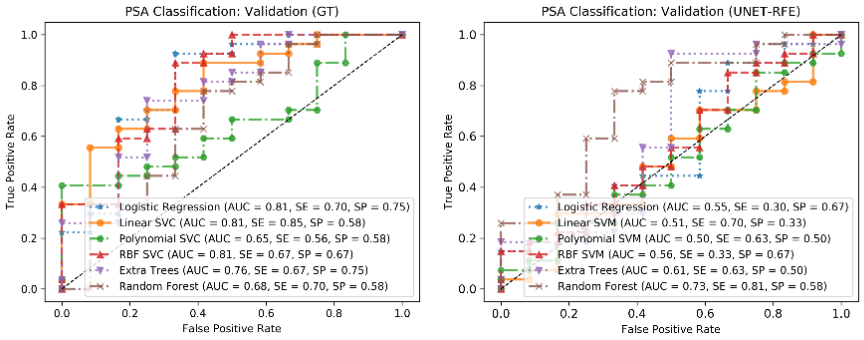

Fig. 5. Receiver operating characteristic (ROC) curves based on GT masks and U-Net predicted masks with feature selection. The 6 classifiers are trained and tuned on the training set and applied to the test set (RBF: radial basis function, RFE: recursive feature elimination, AUC: area under the curve, SE: sensitivity, SP: specificity).

As a result, the best performance in terms of accuracy, precision, recall, and Dice in training and test were observed by the multi-channel model with batch size of 16, 0.99 test accuracy, 0.88 test precision, 0.77 test recall, and 0.82 test Dice. Table 2 compares the achieved performances from the alternative U-Net models and those of 40%-SUV$_{MAX}$ masks. Figure 4 provides a qualitative outline of the segmentation results, comparing original input channels and multi-channel U-Net model prediction. As the results suggest, the U-Net predicted mask performs reasonably well as compared to the GT mask. Moreover, the U-Net prediction outperformed the thresholding based mask, specifically, for the identification of the physiological uptake (e. g., in livers and kidneys) which is considered as one of the challenging tasks for computer based algorithms [27, 28]. Furthermore, the proposed automated segmentation performs well in predicting bone metastasis uptakes.

Table 3. The most relevant radiomics features selected by recursive feature elimination (RFE) from both PET and CT modalities. For more information on the radiomics features, refer to [19] (glrm: gray level run length matrix, glszm: gray level size zone matrix).

Feature Group	Feature Subgroup	Feature Name
pet: diagnostics	Image-original	Mean
pet: original	shape	SurfaceVolumeRatio
ct: original	shape	MinorAxisLength
pet: original	firstorder	Energy
pet: original	firstorder	Maximum
pet: original	firstorder	Skewness
pet: original	glrlm	RunEntropy
pet: original	glrlm	RunLengthNonUniformityNormalized
pet: original	glrlm	RunPercentage
ct: original	glrlm	ShortRunEmphasis
ct: original	glszm	SmallAreaEmphasis
ct: original	glszm	SmallAreaLowGrayLevelEmphasis
pet: original	glszm	ZonePercentage
ct: original	glszm	ZonePercentage

3.2 Therapy Response Prediction

To analyze classifiers' performances, radiomics features have been calculated for both GT and U-Net predicted masks. A total of 120 radiomics features including first and higher-order statistics such as minimum and maximum intensity, textural heterogeneity parameters such as entropy and kurtosis, and run and zone-length statistics are calculated for both PET and CT modalities using PyRadiomics library. For the complete list of the features visit PyRadiomics official documentation [19]. Among all the classifiers, logistic regression performed

the best as applied to the radiomics features calculated based on GT masks with AUC=0.81, SE=0.70, SP=0.75 on the test set. As the prediction performances of all the classifiers as applied to U-Net predicted masks were not satisfactory (AUC ranged from 0.41 to 0.55), recursive feature elimination technique has been applied to identify most relevant features for the classification task. Table 3 shows the list of 14 features as selected by RFE method. Taking advantage of feature selection, the classification performances of most of the classifiers have been clearly improved. As previous work [14, 27] had suggested, features from both PET and CT modalities contribute to the classification task. The overall best performance belongs to random forest classifier with AUC=0.73, SE=0.81, SP=0.58 as applied to the held-out test cohort. Figure 5 shows receiver operating characteristic (ROC) curves for all of the 6 classifiers as applied to radiomics features calculated based on GT and U-Net predicted masks after applying recursive feature elimination (RFE).

4 Discussion

Facilitating fast and accurate non-invasive diagnosis and prognosis has been the objective of computer-aided diagnosis (CAD) for years. When it comes to the oncological domain, especially in subjects in advanced metastatic stages, CAD systems take over the histopathological analyses in many clinical practices. This is globally justified as taking multiple biopsies from patients is ethically questionable. However, the procedure of manual delineation of the malignant tissues using established tools such as InterView FUSION is considered time consuming and attention intensive. Therefore, the first goal of this study was to develop an automated segmentation tool for multimodal PET/CT scans.

We retrospectively analyzed 2067 pathological hotspots from 100 PCa patients (on average, 20 pathological hotspots per patient). As shown in Results section, our U-Net based multi-channel segmentation network predicts the pathological masks with a high accuracy. Particularly, we showed that including the PET and CT modalities as multiple channels outperforms predictions of the U-Net model as trained only using the original PET channel. Also, the qualitative analyses revealed that the multi-channel U-Net prediction is superior in discriminating non-pathological uptake in liver and kidneys compared to 40%-SUV$_{MAX}$ mask as a conventional threshold based method.

Predicting ^{177}Lu-PSMA therapy response has been the second goal of this study. To this end, we calculate radiomics features based on the U-Net predicted masks. As radiomics analysis has been successfully used in many oncological studies for treatment response prediction and analysis of overall survival [5, 14, 29, 30], combining automated segmentation with radiomics analysis for multimodal ^{68}Ga-PSMA-PET/CT findings is another contribution of our method. Results of the classification task confirm the potential of a fully automated approach, even though the comparison to predictions based on manual segmentation still indicates room for improvement. In the future, we plan to explore an end to end prediction of treatment response using a deep neural network.

However, we expect that successfully training such an approach might require a larger cohort.

In this study, we focused on ^{68}Ga-PSMA-PET/CT scans and used a retrospective dataset from a single NM center using a single PET/CT scanner. However, the findings need to be further compared to that of other scanners as well as other biomarkers such as fluorodeoxyglucose (FDG). To improve these preliminary results, both the U-Net based segmentation as well as the radiomics analysis pipelines should be enhanced. Furthermore, to implement decision support tools which can take part in clinical routines in near future, we plan to include PET/CT images from different scanners and centers as well as other biomarkers.

5 Conclusion

Successful prediction of ^{177}Lu-PSMA treatment response would have a major impact on clinical decisions in patients with advanced prostate carcinoma. To our knowledge, we present the first fully automated system for this task. It is based on applying a multi-channel U-Net to multimodal ^{68}Ga-PSMA-PET/CT scans, which automatically delineates pathological uptake with a high accuracy. Supervised machine learning is then applied to radiomics features to predict treatment response. We expect that training data from larger studies will further increase the accuracy achieved by systems like ours, and will permit assessing the generalizability of the results.

6 Data and Code Availability

Due to German regulations on medical data availability, we cannot disclose the data, however all the data would be available for review on-site. The in-house developed code is available online at https://gitlab.com/Moazemi/pet-ct-u-net.

References

1. Ferlay, J., Lam, F., Colombet, M., Mery, L., Pineros, M., Znaor, A., Soerjomataram, I. et al.: Global cancer observatory: cancer today. Lyon, France: International Agency for Research on Cancer. https://gco.iarc.fr/today. Last accessed 30 June 2021).
2. Jin, S., Li, D., Wang, H., Yin, Y.: Registration of PET and CT images based on multiresolution gradient of mutual information demons algorithm for positioning esophageal cancer patients. Journal of Applied Clinical Medical Physics, vol. 14, num. 1, pp. 55–61 (2013). https://doi.org/10.1120/jacmp.v14i1.3931
3. Bundschuh, R.A., Dinges, J., Neumann, L., Seyfried, M., Zsótér, N., Papp, L., Rosenberg, R., Becker, K., and Astner, S.T., Henninger, M., Herrmann, K., Ziegler, S.I., Schwaiger, M., Essler, M.: Textural Parameters of Tumor Heterogeneity in 18F-FDG PET/CT for Therapy Response Assessment and Prognosis in Patients with Locally Advanced Rectal Cancer. Journal of Nuclear Medicine, vol. 55, num. 6, pp. 891–897 (2014). https://doi.org/10.2967/jnumed.113.127340

4. Bang, J.I., Ha, S., Kang, S.B., Lee, K.W., Lee, H.S, Kim, J.S, Oh, H.K., Lee, H.U., Kim, S.E.: Prediction of neoadjuvant radiation chemotherapy response and survival using pretreatment [18F]FDG PET/CT scans in locally advanced rectal cancer. Eur J Nucl Med Mol Imaging, vol. 43, pp. 422431 (2016). https://doi.org/10.1007/s00259-015-3180-9
5. Ypsilantis, P.P., Siddique, M., Sohn, H.M., Davies, A., Cook, G., Goh, V., Montana, G.: Predicting Response to Neoadjuvant Chemotherapy with PET Imaging Using Convolutional Neural Networks. PLoS One. (2015) vol.10 num. 9 https://doi.org/10.1371/journal.pone.0137036
6. Gorgi Zadeh, S., Wintergerst, M., Wiens, V., Thiele, S., Holz, F., Finger, R., Schultz, T.: CNNs Enable Accurate and Fast Segmentation of Drusen in Optical Coherence Tomography. In: Deep Learning in Medical Image Analysis (DLMIA), LNCS 2017, Springer.
7. Selvaganesan, K., Whitehead, E., DeAlwis, P.M., Schindler, M.K., Inati, S., Saad, Z.S., Ohayon, J.E., Cortese, I.C.M., Smith, B., Jacobson, S., Nath, A., Reich, D.S., Inati, S., Nair, g.: Robust, atlas-free, automatic segmentation of brain MRI in health and disease. Heliyon. (2019) vol. 5, num. 2, pp. e01226 https://doi.org/10.1016/j.heliyon.2019.e01226
8. Ronneberger, O., Fischer, P., Brox, T.: U-Net: Convolutional Networks for Biomedical Image Segmentation. In: Navab, N., Hornegger, J., Wells, W., Frangi, A. (eds) Medical Image Computing and Computer-Assisted Intervention MICCAI 2015. MICCAI (2015). Lecture Notes in Computer Science, vol. 9351. Springer, Cham. https://doi.org/10.1007/978-3-319-24574-4_28
9. Hatt, M., Laurent, B., Ouahabi, A., Fayad, H., Tan, S., Li, L., Lu, W., Jaouen, V., Tauber, C., Czakon, J, et al.: The first MICCAI challenge on PET tumor segmentation, Medical Image Analysis, (2018), vol. 44, pp. 177-195, ISSN 1361-8415, https://doi.org/10.1016/j.media.2017.12.007
10. Li, L., Zhao, X., Lu, W., Tan, S.: Deep learning for variational multimodality tumor segmentation in PET/CT, Neurocomputing, (2020) vol. 392, pp. 277-295, ISSN 0925-2312, https://doi.org/10.1016/j.neucom.2018.10.099
11. Liu, L., Cheng, J., Quan, Q., Wu, F.X , Wang, Y. P., Wang, J.: A survey on U-shaped networks in medical image segmentations, Neurocomputing, (2020) vol. 409, pp. 244-258, ISSN 0925-2312, https://doi.org/10.1016/j.neucom.2020.05.070
12. Beukinga, R.J., Hulshoff, J.B.,van Dijk, L.V., Muijs, C.T., Burgerhof, J.G.M., Kats-Ugurlu, G., Slart, R.H.J.A., Slump, C.H.,Mul, V.E.M., Plukker, J.Th.M. et al.: Predicting Response to Neoadjuvant Chemoradiotherapy in Esophageal Cancer with Textural Features Derived from Pretreatment 18F-FDG PET/CT Imaging. Journal of Nuclear Medicine, vol. 58, num. 5, pp. 723729 (2017). https://doi.org/10.2967/jnumed.116.180299
13. Cheng, J. Z., Ni, D., Chou, Y. H., Qin, J., Tiu, C. M., Chang, Y. C., Huang, C. S., Shen, D., Chen, C. M.: Computer-Aided Diagnosis with Deep Learning Architecture: Applications to Breast Lesions in US Images and Pulmonary Nodules in CT Scans. Scientific reports, (2016) vol. 6. https://doi.org/10.1038/srep24454
14. Moazemi, S., Erle, A., Khurshid, Z., Ltje, S., Muders, M., Essler, M., Schultz, T., Bundschuh, R. A.: Decision-support for treatment with 177Lu-PSMA: machine learning predicts response with high accuracy based on PSMA-PET/CT and clinical parameters. Annals of translational medicine, (2021) vol. 9,9, 818. https://doi.org/10.21037/atm-20-6446
15. Parisot, C.: The DICOM standard. Int J Cardiac Imag, (1995) vol. 11, pp. 171177 . https://doi.org/10.1007/BF01143137

16. Abadi, M., Agarwal, A., Barham, P., Brevdo, E., Chen, Z., Citro, C., Corrado, G.S., Davis, A., Dean, J. Devin, M., et al.: TensorFlow: Large-scale machine learning on heterogeneous systems, (2015). tensorflow.org https://doi.org/10.5281/zenodo.4724125
17. Chollet, F.: Keras. GitHub repository. (2015), https://github.com/fchollet/keras
18. Dice, L.R.: Measures of the Amount of Ecologic Association Between Species. Ecology. (1945), vol. 26, num. 3, pp. 297302. https://doi.org/10.2307/1932409. JSTOR 1932409.
19. van Griethuysen, J. J. M., Fedorov, A., Parmar, C., Hosny, A., Aucoin, N., Narayan, V., Beets-Tan, R. G. H., Fillon-Robin, J. C., Pieper, S., Aerts, H. J. W. L.: Computational Radiomics System to Decode the Radiographic Phenotype. Cancer Research. (2017), vol. 77, num. 21, pp. e104e107. https://doi.org/10.1158/0008-5472.CAN-17-0339
20. Guyon, I., Weston, J., Barnhill, S., Vapnik, V.: Gene selection for cancer classification using support vector machines. Mach. Learn. (2002), vol.46, pp. 389422, https://doi.org/10.1023/A:1012487302797
21. Official Company Website for the InterView FUSION: Software. https://www.mediso.de/Interview-fusion.html Last accessed 30 June 2021
22. Tomar, N.K.: Polyp Segmentation using UNET in TensorFlow 2.0. https://idiotdeveloper.com/polyp-segmentation-using-unet-in-tensorflow-2/. Last accessed 30 June 2021).
23. Wright, R. E.: Logistic regression. In Grimm, L.G., Yarnold, P.R.: (eds.), Reading and understanding multivariate statistics, (1995) , pp. 217244. American Psychological Association.
24. Hearst, M.A., Dumais, S.T., Osuna, E., Platt, J., Scholkopf, B.: Support vector machines. IEEE Intelligent Systems and their Applications, (1998), vol. 13, num. 4, pp. 18-28, https://doi.org/10.1109/5254.708428
25. Simm, J., de Abril, I., Sugiyama, M.: Tree-Based Ensemble Multi-Task Learning Method for Classification and Regression, (2014), volume 97 number 6. http://CRAN.R-project.org/package=extraTrees
26. Breiman, L.: Random Forests. Machine Learning, (2001), vol. 45, pp. 532 . https://doi.org/10.1023/A:1010933404324
27. Moazemi, S., Khurshid, Z., Erle, A., Ltje, S., Essler, M., Schultz, T., Bundschuh, R. A.: Machine Learning Facilitates Hotspot Classification in PSMA-PET/CT with Nuclear Medicine Specialist Accuracy. Diagnostics (Basel, Switzerland), (2020) vol. 10,9, 622. https://doi.org/10.3390/diagnostics10090622
28. Erle, A., Moazemi, S., Ltje, S., Essler, M., Schultz, T., Bundschuh, R.A.: Evaluating a Machine Learning Tool for the Classification of Pathological Uptake in Whole-Body PSMA-PET-CT Scans. Tomography (2021) vol. 7, pp. 301-312. https://doi.org/10.3390/tomography7030027
29. Vallieres, M., Kay-Rivest, E., Perrin, L.J., Liem, X., Furstoss, C., Aerts, H., Khaouam, N., Nguyen-Tan, P.F., Wang, C.S., Sultanem, K., Seuntjens, J., El Naqa, I.: Radiomics strategies for risk assessment of tumour failure in head-and-neck cancer. Scientific reports, (2017), vol. 7, num. 1, pp. e10117, https://doi.org/10.1038/s41598-017-10371-5
30. Moazemi, S., Erle, A., Ltje, S., Gaertner, F. C., Essler, M., Bundschuh, R. A.: Estimating the Potential of Radiomics Features and Radiomics Signature from Pretherapeutic PSMA-PET-CT Scans and Clinical Data for Prediction of Overall Survival When Treated with 177Lu-PSMA. Diagnostics (2021) vol. 11,2, 186. https://doi.org/10.3390/diagnostics11020186